Locally Implicit Total-Variation-Diminishing Schemes on Unstructured Triangular Meshes

C. J. Hwang* and J. L. Liu†
National Cheng Kung University, Tainan, Taiwan 70101, Republic of China

A numerical solution procedure that includes locally implicit total-variation-diminishing schemes and adaptive mesh generation techniques has been developed in this work. In a Cartesian coordinate system, the Euler equations are solved by using a cell-centered finite volume algorithm. A new construction of symmetric total-variation-diminishing schemes on unstructured triangular meshes is presented. The validation of the present solution-adaptive methods is confirmed by comparison with related numerical results for inviscid flows around an isolated NACA 0012 airfoil and passing through a channel with a circular arc bump in transonic and supersonic flow regimes. To further prove the feasibility of this approach, a two-element airfoil flow is also investigated. Furthermore, one unsteady transonic channel flow is studied to demonstrate the reliability and capability of the present solution procedure for a time accurate calculation.

Introduction

In recent years, considerable progress has been made in computational aerodynamics. The use of triangular meshes to solve the Euler equations over arbitrary geometries has gained significant attention.[1-4] Two major reasons for using the unstructured triangular meshes are 1) flow regions with complex geometries can be easily discretized; and 2) flow features are simulated correctly on the appropriate distribution of grid points by solution-adaptive methods. In this work, the unstructured triangular meshes are generated, and solution-adaptibility are obtained by the remeshing and refinement techniques.

Numerical methods for compressible inviscid flows fall into three major classes: finite difference, finite volume, and finite element methods. The main advantage of cell-centered finite volume algorithms over finite difference and finite element methods is that less effort is needed to treat singular points. To achieve the solutions of internal and external flows, many explicit and implicit algorithms have been presented to solve the compressible Euler equations. On the unstructured meshes, explicit four- or five-stage Runge-Kutta time integration has been widely employed.[2-4] This scheme is reliable and efficient to implement for numerical calculations. On the unstructured meshes, several fully implicit schemes have been developed.[4-6] They are not bounded by stability limitations, and the solutions are obtained by a large system of algebraic equations. For the triangular meshes, Slack et al.[4] used a reverse Cuthill-McGee renumbering scheme as a preprocessor for LU decomposition to reduce the requirements of storage and CPU time. As mentioned in Ref. 5, Venkatakrishnan and Barth introduced a Newton iteration and a minimum degree algorithm to solve the sparse matrix. It is found that the time taken to order the grid points by the minimum degree algorithm is less than 10% of the time required for the factorization. In order to have the same level of implicitness for all polygonal cells, Struijs et al.[6] imposed a suitable sweep-pattern to renumber the grid cells, and the point Gauss-Seidel relaxation was implemented. Free of any matrix system solvers, a modified Gauss-Seidel scheme has been proposed by Reddy and Jacocks[7] to study steady solutions of inviscid airfoil flows on structured quadrilateral meshes. The scheme is locally implicit but globally explicit, and is unconditionally stable under local linearization of analysis. As mentioned in Ref. 8, the scheme has the following features: 1) computational efficiency to minimize the arithmetic operations; 2) adaptability to computational domains consisting of either blocked or nonstructured grids; 3) fast convergence; and 4) numerical reliability (i.e., robustness). Without renumbering the cells and using any matrix system solvers, this kind of time integration technique is extended for symmetric sweeps on unstructured triangular meshes in the present paper.

Jameson and Mavriplis[1,2] developed an explicit finite volume algorithm for cell-centered and nodal schemes to solve the Euler equations on triangular meshes. These schemes contain adaptive dissipation terms and have been found to give good results for flows past a variety of configurations. It is known that the dissipation model requires two coefficients which are determined empirically. To avoid choice of those two constants by user input, a total-variation-diminishing (TVD) scheme is introduced in this paper. In structured quadrilateral grid systems, Yee[9,10] has modified and generalized Harten's second-order TVD scheme to explicit and implicit non-MUSCL-type approaches for steady-state as well as unsteady flow calculations. The advantages that symmetric TVD schemes provide over upwind TVD schemes are 1) reduced computational effort, 2) a more natural way of extending the scheme to two- and three-dimensional problems, and 3) less sensitive to the boundary conditions treatment. These features have been mentioned in related papers by Yee, Harten, and Moon.[9-11] In this paper, a new construction of

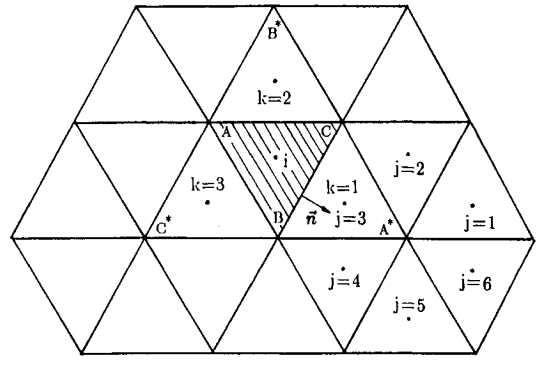

Fig. 1 Definition of unstructured triangular mesh for the cell-centered TVD scheme.

Received Feb. 26, 1990; revision received Aug. 7, 1990; accepted for publication Aug. 13, 1990. Copyright © 1990 by the American Institute of Aeronautics and Astronautics, Inc. All rights reserved.

*Associate Professor, Institute of Aeronautics and Astronautics. Member AIAA.
†Graduate Student.

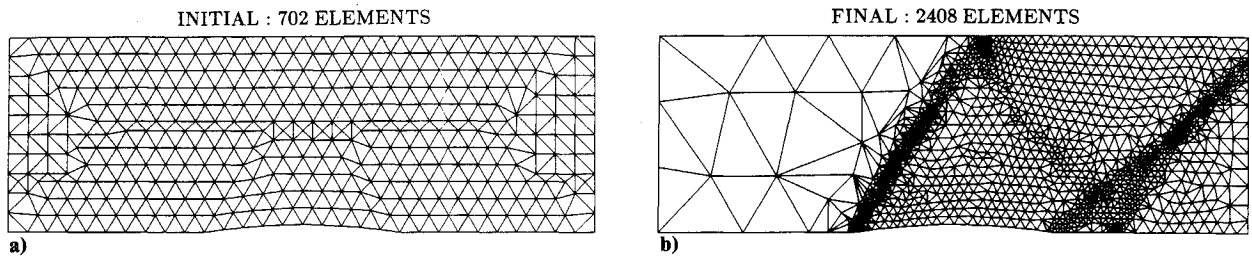

Fig. 2 Flow passing through channel with 4% thick circular arc bump ($M_\infty = 1.4$): a) initial; b) final meshes.

symmetric TVD schemes on unstructured triangular meshes in a Cartesian coordinate system is developed and applied to two-dimensional steady and unsteady flow calculations.

The purpose of this work is to create and demonstrate a numerical solution procedure for studying two-dimensional compressible inviscid flows. The procedure includes 1) cell-centered, finite volume, symmetric TVD formulation on a triangular mesh, 2) adaptive mesh generation, and 3) locally implicit time integration. The Euler equations are solved on unstructured triangular meshes. To evaluate the present approach, the inviscid flows passing through a channel with a circular arc bump and around single- as well as two-element airfoils are studied. Finally, the numerical method is applied to a two-dimensional unsteady transonic flow for a channel with time-varying back pressure. By comparing with the related numerical results, the present solution procedure is proved to be accurate, reliable, and suitable for the flows with complex phenomena or geometries.

Governing Equations

By choosing the chord length c and flow properties at inlet or freestream stagnation condition as reference variables, the two-dimensional unsteady continuity, momentum and energy equations are written in nondimensional form for the Cartesian coordinate system as follows:

$$\frac{\partial U}{\partial t} + \frac{\partial E}{\partial x} + \frac{\partial G}{\partial y} = 0 \tag{1}$$

where

$$U = \begin{bmatrix} \rho \\ \rho u \\ \rho v \\ e \end{bmatrix}, \quad E = \begin{bmatrix} \rho u \\ \rho u^2 + P \\ \rho uv \\ (e + P)u \end{bmatrix}, \quad G = \begin{bmatrix} \rho v \\ \rho uv \\ \rho v^2 + P \\ (e + P)u \end{bmatrix}$$

The unknown variables ρ, u, v, and e represent the gas density, velocity components in x,y directions and total energy per unit volume. In this paper, the working fluid is air, and it is assumed to be perfect. That is, the pressure P is given by the equation of state

$$P = (\gamma - 1)\,[e - (\rho/2)(u^2 + v^2)] \tag{2}$$

where γ is the ratio of specific heats and typically taken as 1.4 for air.

Numerical Algorithm

The governing equations in Eq. (1) can be rewritten as

$$\frac{\partial U}{\partial t} + (\nabla \cdot F) = 0 \tag{3}$$

where F represents the convective flux vector. By integrating Eq. (3) over space and using the Gauss theorem, the following expression is obtained:

$$\frac{\partial}{\partial t}\int\int_\Omega U\,dA + \int_{\partial\Omega} F \cdot dl = 0 \tag{4}$$

where $dl = n\,dl$, and n is the unit normal vector in the outward direction. The variable Ω is the domain of computation and $\partial\Omega$ the boundary of the domain. A two-parameter family of TVD schemes for each triangular cell i (Fig. 1) can be written as

$$A_i\left(\frac{U^{n+1} - U^n}{\Delta t}\right)_i + \frac{\theta}{1+\beta} Q_i(U^{n+1})$$

$$= -\frac{1-\theta}{1+\beta} Q_i(U^n) + \frac{\beta}{1+\beta}\left(\frac{A}{\Delta t}\right)_i (U_i^n - U_i^{n-1}) \tag{5}$$

where $0 \le \theta \le 1$ and $-\frac{1}{2} \le \beta \le \frac{1}{2}$. This two-parameter family of TVD schemes consists of implicit ($\theta \neq 0$) as well as explicit ($\theta = 0$) schemes. In this paper, we choose $\theta = 1$ and $\beta = 0$ for steady-state flow calculations that are first-order accurate in time. For unsteady computations, $\theta = 1$ and $\beta = \frac{1}{2}$ are used and the scheme becomes second-order accurate in time. Choosing the parameter θ equal to one, the CFL-like (Courant-Friedrichs-Lewy) restriction for TVD sufficient conditions related to time is eliminated, and the schemes are unconditionally TVD.[9] It may be noted that Eq. (5) is TVD for the "locally frozen" constant coefficient system, and then applied in a scalar form to each characteristic field. The matrix R_{ik} is the eigenvector of the Jacobian matrix $[(\partial F/\partial U)\cdot dl]_{ik}$ on the interface between cell i and cell k, and R_{ik}^{-1} is the inverse matrix of R_{ik}. The numerical flux function Q_i in Eq. (5) for non-MUSCL-type symmetric TVD schemes in a Cartesian coordinate system is expressed as

$$Q_i(U) = \frac{1}{2}\sum_{k=1}^{3}[(F_i + F_k)\cdot dl_{ik} - R_{ik}\Phi_{ik}] \tag{6}$$

where R_{ik} is evaluated by Roe's average, and Φ_{ik} is defined as

$$\Phi_{ik} = \Psi(\Lambda_{ik})[\Delta\alpha_{ik} - \Delta\tilde{\alpha}_{ik}] \tag{7}$$

The matrix $\Delta\alpha_{ik}$ has the elements of $R_{ik}^{-1}(U_k - U_i)$, and Λ_{ik} are eigenvalues of matrix $[(\partial F/\partial U)\cdot dl]_{ik}$. The function Ψ is defined as

$$\Psi(z) = \begin{cases} |z| & \text{if } |z| \ge \epsilon; \\ (z^2 + \epsilon^2)/2\epsilon & \text{otherwise} \end{cases} \tag{8}$$

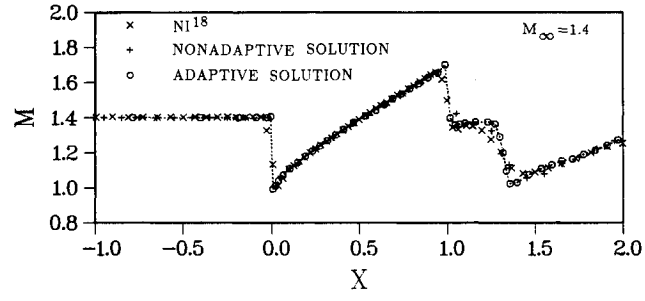

Fig. 3 Mach number distributions for inviscid flow passing through channel with 4% thick circular arc bump ($M_\infty = 1.4$).

where $\Psi(z)$ in Eq. (8) is an entropy correction to $|z|$, and ϵ is a small positive parameter. The "limiter" function $\Delta\bar{\alpha}_{ik}$ can be expressed as

$$\Delta\bar{\alpha}_{ik} = \text{minmod}(\Delta\alpha_{ik},\ \Delta\alpha_{ik}^{+},\ \Delta\alpha_{ik}^{-}) \tag{9}$$

where $\Delta\alpha_{ik}^{+} = R_{ik}^{-1}(U_L{}^* - U_{ik})$, $\Delta\alpha_{ik}^{-} = R_{ik}^{-1}(U_{ik} - U_L)$, and L is the index of A, B, or C. For instance, $L = A$ for $k = 1$ is shown in Fig. 1. The value of the minmod function is equal to the smallest number in absolute value if the list of arguments is of the same sign, or is equal to zero if any arguments are of opposite sign. The use of a limiter reduced the order of accuracy of the interpolation to first-order near regions of large gradients in order to suppress oscillations near discontinuities, while maintaining second-order accuracy in smooth regions. In this paper, the interpolation is accomplished by choosing the properties at cell center and nodal points shown in Fig. 1. At the nodes, the properties are obtained by the area-weighting rule. For example, the quantity $U_A{}^*$ (Fig. 1) can be written as

$$U_A{}^* = \left(\sum_{j=1}^{6} U_j A_j\right) \Big/ \left(\sum_{j=1}^{6} A_j\right) \tag{10}$$

By using the Taylor series expansion for the temporal difference, Eq. (5) is linearized and can be constructed in the delta form as follows:

$$L_i(\Delta U) = \text{Res}_i^n = -\frac{1}{1+\beta} Q_i(U^n) + \frac{\beta}{1+\beta}\left(\frac{A}{\Delta t}\right)_i (U_i^n - U_i^{n-1}) \tag{11}$$

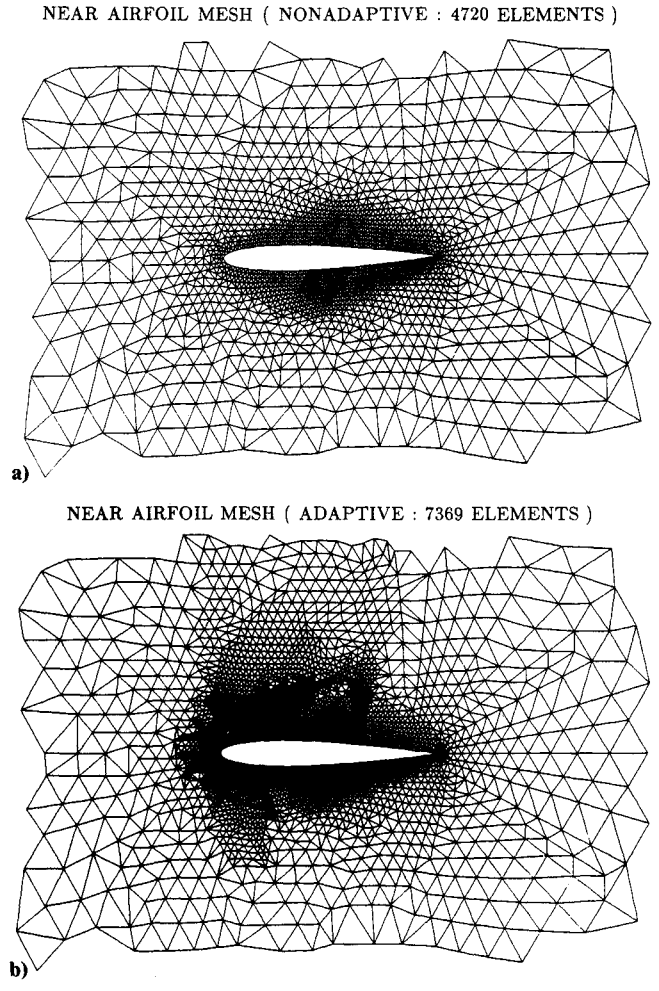

Fig. 4 Partial view of meshes for the NACA 0012 airfoil: a) nonadaptive; b) adaptive.

where

$$L_i(\Delta U) = CI\Delta U_i + CK_1\Delta U_1 + CK_2\Delta U_2 + CK_3\Delta U_3$$

and

$$CI = \left(\frac{A}{\Delta t}\right)_i + \frac{\theta}{2(1+\beta)}\sum_{k=1}^{3}\left\{M_{ik} + R_{ik}\Psi(\Lambda_{ik})R_{ik}^{-1}\left(1 - \frac{\Delta\bar{\alpha}_{ik}}{\Delta\alpha_{ik}}\right)\right\}$$

$$CK_L = \frac{\theta}{2(1+\beta)}\left\{M_{iL} - R_{iL}\Psi(\Lambda_{iL})R_{iL}^{-1}\left(1 - \frac{\Delta\bar{\alpha}_{iL}}{\Delta\alpha_{iL}}\right)\right\}, L = 1,2,3$$

$$M_{ik} = \left(\frac{\partial \boldsymbol{F}}{\partial U}\cdot \mathrm{d}\boldsymbol{l}\right)_{ik}$$

To solve Eq. (11), a modified Gauss-Seidel scheme is employed. This algorithm is based on two relaxation procedures for solving time-dependent partial differential equations.[7] The scheme is locally implicit, but globally explicit and is unconditionally stable under local linearized analysis.[8] It does not require the assembly of any global matrices and does not need any matrix system solvers. In this paper, the technique is

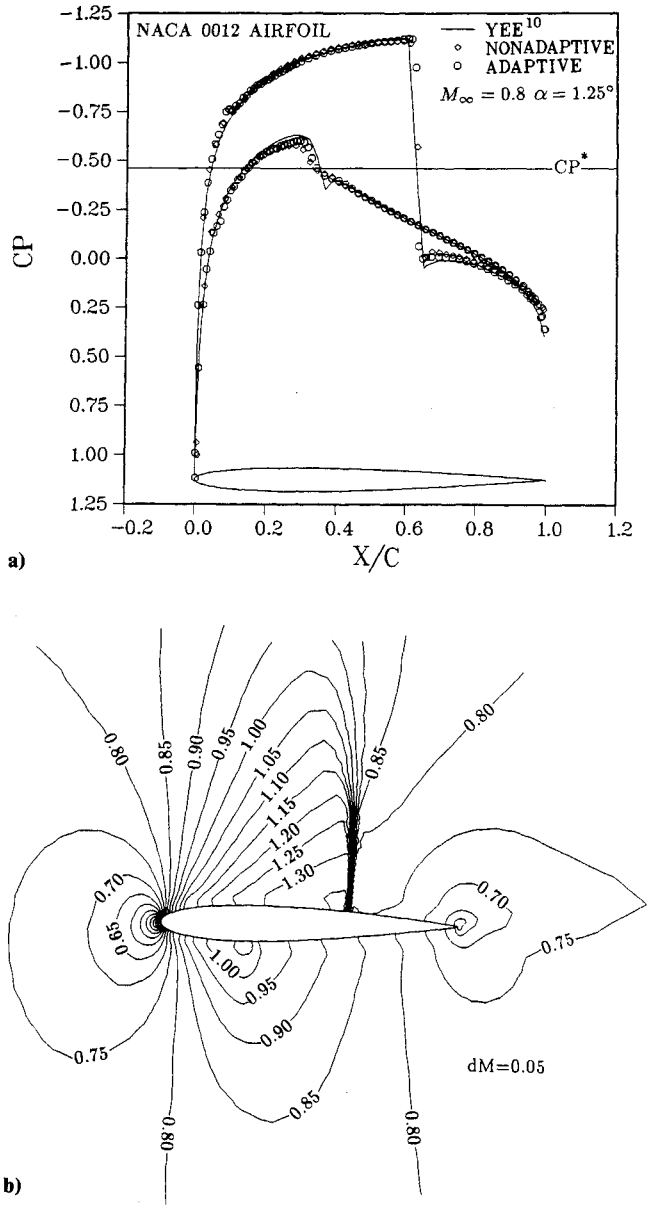

Fig. 5 Inviscid flow over the NACA 0012 airfoil ($M_\infty = 0.8$, $\alpha = 1.25$ deg): a) pressure coefficient distribution; b) Mach number contours.

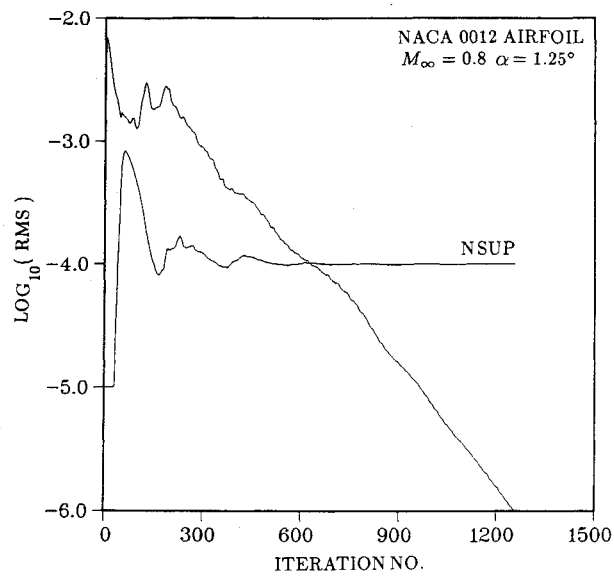

Fig. 6 Convergence history for inviscid flow over the NACA 0012 airfoil ($M_\infty = 0.8$, $\alpha = 1.25$ deg).

extended to unstructured triangular meshes. The calculation for a symmetric cycle of inner iterative corrections is performed by starting at the first element and sweeping to the latest element followed by an opposite sweep. Thus, for each cell i, the equations are written as

$$CdU_i = \mathrm{Res}_i^n - L_i(\Delta U) \tag{12}$$

$$\Delta U_i^{(m+1)} = \Delta U_i^{(m)} + w_{\mathrm{in}} dU_i, \qquad m = 1,2 \tag{13}$$

where matrix C is approximated as a diagonal matrix, which is derived from a modification to the coefficient matrix CI.

$$C = \left\{\left(\frac{A}{\Delta t}\right)_i \left[1.0 + \frac{\theta}{2(1+\beta)} CFL\right]\right\} I \tag{14}$$

where $I = \mathrm{Diag}[1, 1, 1, 1]$ and CFL is the Courant-Friedrichs-Lewy number. The variable ΔU shown on the right-hand side of Eq. (12) takes the latest available values from Eq. (13). It may be noted that the dissipation terms shown in matrix CI have not been introduced in Eq. (14). This kind of treatment does not affect the solutions of steady and unsteady flows. The inner iteration for $\Delta U_i^{(m+1)}$ can be computed rapidly since the correction dU_i is obtained from explicit scalar equations. One symmetric cycle of inner iterations is employed in each time step for steady-state flows, while several cycles are performed until a convergence state of $\Delta U_i^{(m+1)}$ is reached for unsteady flow calculations. At the end of a time step, the outer relaxation is introduced

$$U_i^{n+1} = U_i^n + w_{\mathrm{out}} \Delta U_i \tag{15}$$

By incorporating a smoothing process to ΔU implicitly, the iterative process can be made more robust, and convergence to the steady-state solution is speeded up by allowing over-relaxation.[8] In the present work, the smoothing term $\bar{L}_i(\Delta U)$, that is expressed as an undivided Laplacian operator and added to $L_i(\Delta U)$ in Eq. (11), is given as

$$\bar{L}_i(\Delta U) = -w_{\mathrm{imp}}(\psi_{i1}\Delta U_1 + \psi_{i2}\Delta U_2 + \psi_{i3}\Delta U_3 - \sum_{k=1}^{3} \psi_{ik}\Delta U_i) \tag{16}$$

and a diagonal matrix $\bar{C}$ is added to C in Eq. (14),

$$\bar{C} = \left(0.5 w_{\mathrm{imp}} \sum_{k=1}^{3} \psi_{ik}\right) I \tag{17}$$

The quantity ψ_{ik}, shown in Eqs. (16) and (17), is the spectral radius of M_{ik} and is expressed as follows:

$$\psi_{ik} = [|V \cdot \mathrm{d}l| + a\,|\mathrm{d}l|]_{ik} \tag{18}$$

where V is the velocity vector and a is the sonic speed. The coefficients w_{in} and w_{out} in Eqs. (13) and (15) are inner and outer relaxation parameters of the order 1.2 (over-relaxation), while w_{out} in Eq. (15) is chosen as 1.0 for unsteady flow computation. The coefficient w_{imp} in Eqs. (16) and (17) is an implicit smoothing parameter of the order 0.1. It may be noted that the implicit smoothing terms do not affect the solution in the steady-state since the residual terms are not altered.

Boundary Conditions

At the body or wall surface, a no-penetration condition is imposed for the inviscid flow. The pressure is estimated by using x- and y-momentum equations. This value is obtained by the following equation[1]:

$$\rho(y_\eta u - x_\eta v)(y_\xi u_\xi - x_\xi v_\xi) = (x_\xi^2 + y_\xi^2)P_\eta - (x_\xi x_\eta + y_\xi y_\eta)P_\xi \tag{19}$$

where ξ and η represent the coordinate lines aligned and normal to the boundary. For the meshes with smooth distribution of regular triangles, the wall pressure is well predicted by using this equation. When the skew meshes are distributed on the body surface, the even-odd oscillations may happen. As mentioned in Ref. 2, the combination of a strong formulation (setting the velocities tangential to the wall and the fluxes through the wall are also set to zero) and the increased connectivity of the triangular meshes inhibit even-odd decoupling of

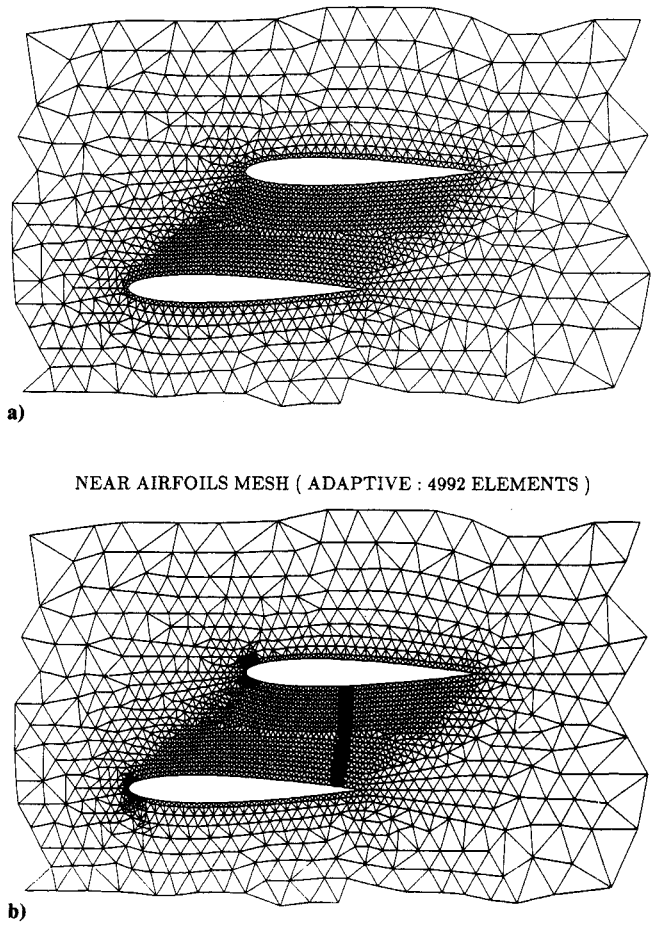

Fig. 7 Partial view of a) nonadaptive and b) adaptive meshes for inviscid flow over staggered biplane ($M_\infty = 0.7$, $\alpha = 0.0$ deg).

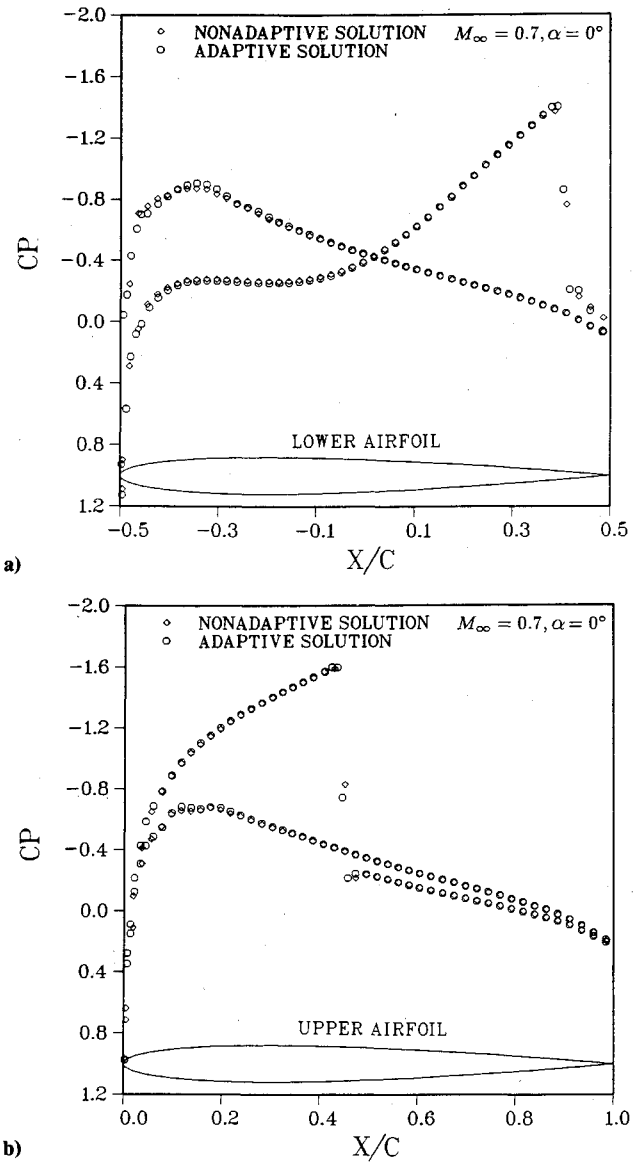

Fig. 8 Pressure coefficient distributions of a) upper and b) lower airfoils for inviscid flow over staggered biplane ($M_\infty = 0.7$, $\alpha = 0.0$ deg).

the solution, and a numerical treatment of artificial dissipation terms on the boundary nodes is also described. It is well known that no dissipation is performed on boundary points for cell center scheme. To reduce the numerical oscillations on body surface, a small value of dissipation is required. In this work, the modified form of Eq. (19) is expressed as

$$\rho(y_\eta u - x_\eta v)(y_\xi u_\xi - x_\xi v_\xi)$$
$$= (x_\xi^2 + y_\xi^2)(P_\eta - D_{art}) - (x_\xi x_\eta + y_\xi y_\eta)(P_\xi - D_{tvd}) \qquad (20)$$

where D_{art} and D_{tvd} are nonlinear fourth-order artificial dissipation and TVD flux correction terms for pressure, respectively. The mathematical forms of D_{art} and D_{tvd} were described in Refs. 1 and 9. In this paper, the Eq. (20) is performed only for the single and two-element airfoils flows after meshes are refined. For the supersonic flows, the freestream conditions are specified at the inflow boundary, and zero-order space extrapolation is applied on the exit plane. For the subsonic flow, one-dimensional characteristics are used to treat the upstream and downstream conditions. About the unsteady channel flow, the back pressure is imposed as a function of time.

Adaptive Mesh Generation Techniques

To achieve the adaptive solutions, various grid adaption methods, such as mesh refinement[2,12-14] and remeshing,[15] have been developed. In the present work, the refinement[14] and remeshing techniques are used for steady flow problems. The grid generation processes for triangular meshes include mainly 1) a two-step strategy for distribution of nodes, and 2) triangulation according to the already distributed interior and boundary nodes. In this work, two steps are employed to decide the distribution of nodes. In the first step, the idea of front[16] is used to obtain the positions of nodes. After the rough distribution of nodes has been set up, the second step is introduced. In this step, six candidate nodes surrounding the given node i are generated by equal distribution on the perimeter of circle with radius δ_i, where the node spacing δ_i is provided by the flow solutions on the background mesh. The indicator for mesh regeneration is decided by the first difference of density. Based on the indicator on the background grid, the triangular meshes are reconstructed. The detailed

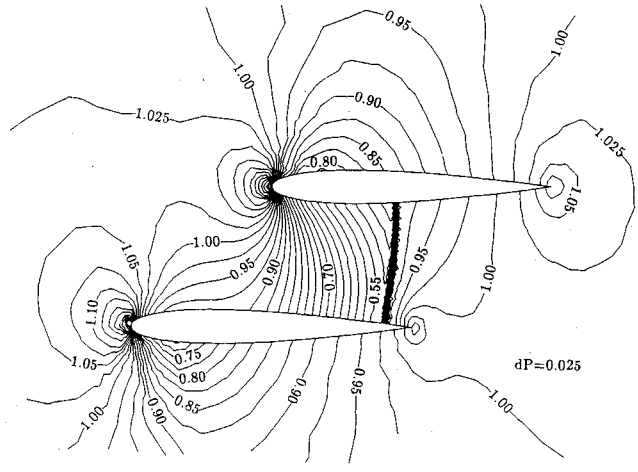

Fig. 9 Pressure contours for inviscid flow over staggered biplane ($M_\infty = 0.7$, $\alpha = 0.0$ deg).

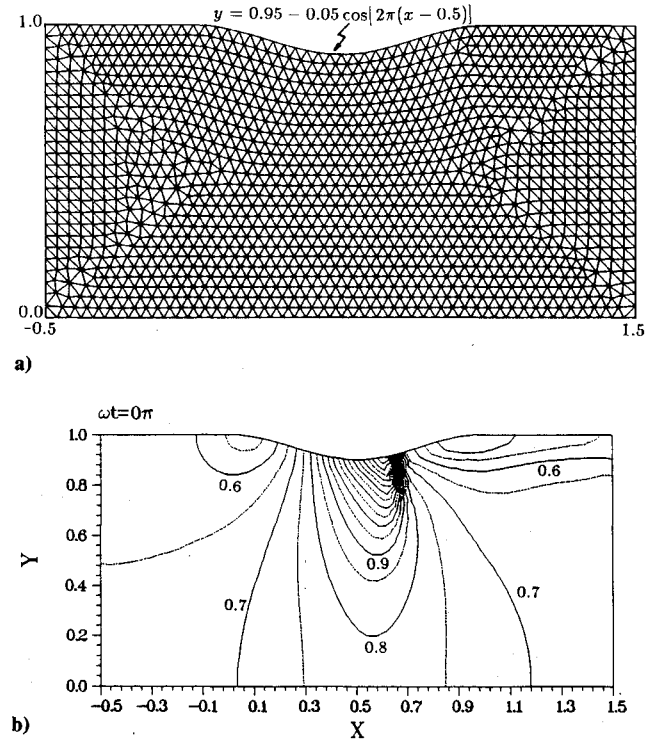

Fig. 10 Channel with a sinusoidal shape: a) uniform mesh; b) Mach number contours for steady state flow ($M_\infty = 0.675$).

descriptions of the earlier adaptive mesh generation techniques are given by Hwang et al.[17] In the present paper, a smoothing process[16] is employed after triangulation, and it is done by shifting each interior generated node to the center of the surrounding polygon.

Results and Discussion

The approach described in the previous section is applied to compute inviscid flows through different regimes (transonic and supersonic flows). Comparing with the related data, the present solution procedure is proved to be accurate and reliable for studying the steady-state and unsteady flows.

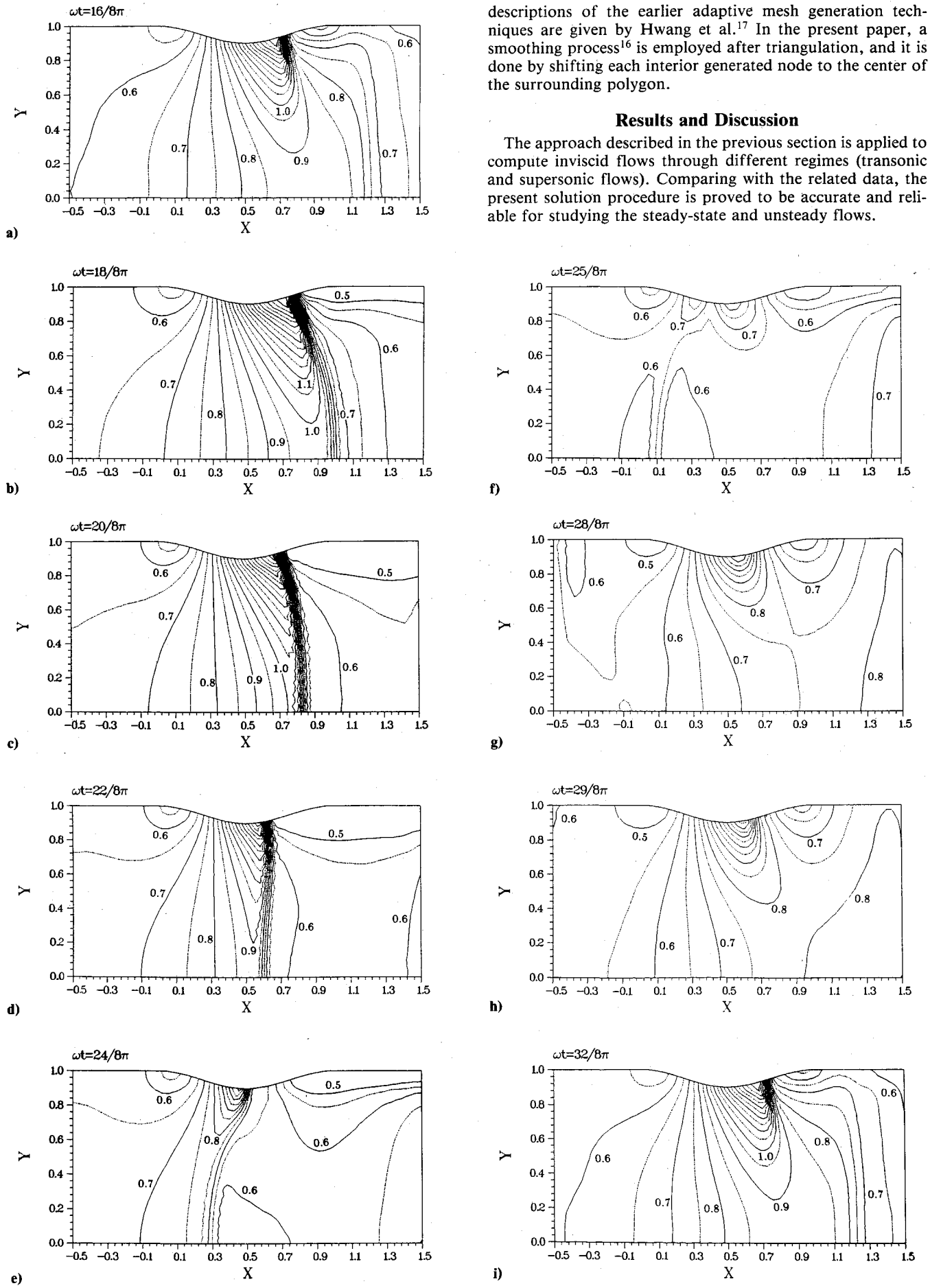

Fig. 11 The sequence of Mach number contours for inviscid flow through channel with time-varying back pressure.

Channel and Isolated Airfoil Flows

To evaluate the present solution procedure, inviscid flows passing through a channel with a circular arc bump and around a NACA 0012 airfoil are investigated. First, a channel with 4% bump thickness ratio is considered. For a supersonic flow ($M_\infty = 1.4$), the initial and final meshes and Mach number distributions are presented in Figs. 2 and 3. As shown in Fig. 2b, the grid distribution clearly indicated the shock location. Comparing the final mesh with that of Ref. 6, the same complex shock structure is easily determined. In Ref. 6, Struijs et al. developed an implicit upwind relaxation solver, and the mesh is generated by the grid enrichment technique based on the pressure or streamwise entropy gradients. From the Mach number distributions shown in Fig. 3, the accurate and high-resolution results are obtained. In this computation, four times remeshing steps are used and the *CFL* number is equal to 20.

After finishing the numerical study of internal flow, the transonic flow ($M_\infty = 0.8$) around an isolated NACA 0012 airfoil with angle of attack ($\alpha = 1.25$ deg) is studied. By using the mesh generation procedure described in the previous section, the initial grid distribution is depicted in Fig. 4a. The outer boundary is located at 20 chord lengths away from the airfoil. By using mesh refinement in this calculation, a total of 7369 elements are employed (Fig. 4b). The finer cells appear around the leading edge, trailing edge, and the shock regions, which locate on upper and lower surfaces of airfoil. As shown in Fig. 5, the pressure coefficient distributions and Mach number contours exhibit a good comparison with Yee's TVD results[10] in which 249×41 quadrilateral points were used. From the convergence history and normalized supersonic points given in Fig. 6, the characteristics of the present solution algorithm are further understood. In this computation, the *CFL* number is chosen as 10.

Two-Element Airfoil Flow

To demonstrate the ability of the present solution procedure for computing flow passing through the complex geometry, a two-element airfoil flow is investigated in this work. The transonic flow considered here is a staggered biplane configuration (Fig. 7a). The calculation is carried out for the lower airfoil half chord apart from the upper airfoil. Although the flow condition is subcritical for a single NACA 0012 airfoil at Mach number equal to 0.7 and zero angle of attack, a shock forms between the two airfoils. The strength of the shock is dependent on the relative positions of the two airfoils. By using the mesh refinement, a shock is obviously observed from the grid distribution shown in Fig. 7b. The pressure coefficient distributions for the individual airfoils are given in Fig. 8, and pressure contours were indicated in Fig. 9. It is apparent that a sharper shock is observed from the adaptive solution. Except for the inner surfaces between the two airfoils, the pressure distributions on the outer surfaces are similar to those of the single airfoil.

Unsteady Transonic Channel Flow

To further understand the reliability and capability of the present method for a time accurate calculation, one unsteady two-dimensional channel flow is introduced. The channel consists of a length of 2.0 and a width of 1.0, with a 10% thick bump on the upper surface. The chord length of the bump is identical to the channel width, and the geometrical shape has a sinusoidal form given in Fig. 10a. The flow is considered here with a steady-state exit pressure of $P_s = 0.7369$, which corresponds to an inlet Mach number of $M_\infty = 0.675$ (Ref. 18). After the steady-state solution has been obtained, the unsteadiness is introduced by varying the exit back pressure according to

$$P = P_s + P_{\text{amp}} \sin[\omega(t - t_0)] \tag{21}$$

where P_{amp} is the amplitude pressure equal to 0.12. In Eq. (21), $\omega/2$ is the nondimensional reduced frequency of the exit pressure fluctuation equal to 0.396, and t_0 is the reference time level taken as zero in the present work. Based on the flux vector splitting finite difference approach, this flow problem was studied in Ref. 19, in which 60×14 quadrilateral cells were employed. On the fixed mesh with 2644 triangles (Fig. 10a), the unsteady phenomenon is investigated by using the presently developed TVD scheme with a *CFL* number of 5.0.

Choosing the steady-state solution (Fig. 10b) as the initial condition, the numerical results related to the oscillating back pressure during the second cycle of motion ($\omega t = 2\pi$ to $\omega t = 4\pi$) are selected for discussion. The solutions of unsteady sequences are displayed in Fig. 11. After finishing the first cycle calculation at $\omega t = (16/8)\pi$ (Fig. 11a), the back pressure values repeat and begin to increase. The Mach number contours at the neighborhood of the exit are pushed upstream. A compression shock occurs at the lower wall, which occupies the whole channel width and forms a choked flow (Figs. 11b). At $\omega t = (20/8)\pi$, the exit pressure has reached a maximum value (Fig. 11c), whereafter it starts to decrease. Since the finite-rate propagation of the pressure disturbance signals, the flow does not react instantaneously, and flow velocity continues to decrease. The lower wall shock still propagated upstream, but the maximum preshock Mach number decreases rapidly as the shock moves upstream (Fig. 11d). The shock at the lower wall is pushed farther into the subsonic region of the channel, and becomes weaker because of the decrease in upstream flow velocity. At the same time, the upper wall shock also is moved upstream, although the steady-state exit pressure is reached (Fig. 11e). The flow is now subsonic throughout the channel, and a small unsteady wave is still being propagated upstream (Fig. 11f). As the imposed pressure wave train approaches the bump, the flow is accelerated to supersonic value at the upper wall. At time $\omega t = (28/8)\pi$ (Fig. 11g), the exit pressure has reached its minimum level. The pressure at the outlet is now increasing, but the shock steepens gradually. Simultaneously, the flow velocity increases at the lower wall (Fig. 11h). The second cycle (2π to 4π) is finished when $\omega t = (32/8)\pi$ is reached. The same flow structure of shock (Fig. 11i) builds itself up as seen at $\omega t = (16/8)\pi$, whereafter the flow pattern will be repeated again.

Conclusions

The locally implicit, cell-centered, finite volume TVD schemes for numerical integration of the Euler equations have been developed on unstructured triangular meshes in a Cartesian coordinate system. To simulate the flow features in an efficient and correct way, the remeshing and refinement techniques are employed to create the solution-adaptive meshes. For the transonic and supersonic flows, which include internal flow passing through a channel with a circular arc bump and external flow around a NACA 0012 airfoil, the accuracy, reliability and convergence of the present solution procedure are confirmed by comparing the computational results with related data. To prove the feasibility of this approach, transonic flow around a two-element airfoil is investigated. For a transonic channel with a time-varying back pressure, the Mach number contours at time sequences are obtained, and those results are almost consistent with physical behaviors, which have been mentioned in Ref. 19. From the numerical experiments in this work, the presently developed locally implicit symmetric TVD schemes on unstructured triangular meshes are shown to be accurate and suitable for studying two-dimensional compressible inviscid steady and unsteady flows with complex phenomena or geometries.

References

[1]Jameson, A., and Mavriplis, D. J., "Finite Volume Solution of the Two-Dimensional Euler Equations on a Regular Triangular Mesh," *AIAA Journal*, Vol. 24, No. 4, 1986, pp. 611–618.

[2]Mavriplis, D. J., "Accurate Multigrid Solution of the Euler Equa-

tions on Unstructured and Adaptive Meshes," *AIAA Journal,* Vol. 28, No. 2, 1990, pp. 213–221.

[3]McGrory, W. D., Walters, R. W., and Lohner, R., "A Three-Dimensional Space Marching Algorithm for the Solution of the Euler Equations on Unstructured Grids," AIAA Paper 90-0014, Jan. 1990.

[4]Slack, D. C., Walters, R. W., and Lohner, R., "An Interactive Adaptive Remeshing Algorithm for the Two-Dimensional Euler Equations," AIAA Paper 90-0331, Jan. 1990.

[5]Venkatakrishnan, V., and Barth, T. J., "Application of Direct Solvers to Unstructured Meshes for the Euler and Navier-Stokes Equations Using Upwind Schemes," AIAA Paper 89-0364, Jan. 1989.

[6]Struijs, R., Vankeirsbilck, P., and Deconinck, H., "An Adaptive Grid Polygonal Finite Volume Method for the Compressible Flow Equations," AIAA Paper 89-1959-CP, June, 1989.

[7]Reddy, K. C., and Jacocks, J. L., "A Locally Implicit Scheme for the Euler Equations," AIAA Paper 87-1144, June, 1987.

[8]Reddy, K. C., and Benek, J. A., "A Locally Implicit Scheme for 3-D Compressible Viscous Flows," AIAA Paper 90-1525, June 1990.

[9]Yee, H. C., "Construction of Explicit and Implicit Symmetric TVD Schemes and Their Applications," *Journal of Computational Physics,* Vol. 68, Jan. 1987, pp. 151–179.

[10]Yee, H. C., and Harten, A., "Implicit TVD Schemes for Hyperbolic Conservation Laws in Curvilinear Coordinates," *AIAA Journal,* Vol. 25, No. 2, 1987, pp. 266–274.

[11]Moon, Y. J., and Yee, H. C., "Numerical Simulation by TVD Schemes of Complex Shock Reflections from Airfoils at High Angle of Attack," AIAA Paper 87-0350, Jan. 1987.

[12]Berger, M. J., and Oliger, J., "Adaptive Mesh Refinement for Hyperbolic Partial Differential Equations," *Journal of Computational Physics,* Vol. 53, March 1984, pp. 484–512.

[13]Dannenhoffer, J. F., and Baron, J. R., "Grid Adaptation for the 2-D Euler Equations," AIAA Paper 85-0484, Jan. 1985.

[14]Lohner, R., Morgan, K., and Zienkiewicz, O. C., "An Adaptive Finite Element Procedure for Compressible High Speed Flows," *Computer Methods in Applied Mechanics and Engineering,* Vol. 51, Sept. 1985, pp. 441–465.

[15]Peraire, J., Vahdati, M., Morgan, K., and Zienkiewicz, O. C., "Adaptive Remeshing for Compressible Flow Computations," *Journal of Computational Physics,* Vol. 72, Oct. 1987, pp. 449–466.

[16]Lo, S. H., "A New Mesh Generation Scheme for Arbitrary Planar Domains," *International Journal for Numerical Methods in Engineering,* Vol. 21, Aug. 1985, pp. 1403–1426.

[17]Hwang, C. J., Wu, S. J., and Sun, Z. Y., "Application of Adaptive Finite Element Methods to the Euler Equations," *Proceedings of the Seventh International Conference on Finite Element Methods in Flow Problems,* April 1989, pp. 99–104.

[18]Ni, R. H., "A Multiple-Grid Scheme for Solving the Euler Equations," *AIAA Journal,* Vol. 20, No. 11, 1982, pp. 1565–1571.

[19]Bolcs, A., Fransson, T. H., and Platzer, M. F., "Numerical Simulation of Inviscid Transonic Flow Through Nozzles with Fluctuating Back Pressure," *ASME Journal of Turbomachinery,* Vol. 111, April 1989, pp. 169–180.